PAPER • OPEN ACCESS

Geometric signatures of tissue surface tension in a three-dimensional model of confluent tissue

To cite this article: Preeti Sahu *et al* 2021 *New J. Phys.* **23** 093043

New Journal of Physics
The open access journal at the forefront of physics

Deutsche Physikalische Gesellschaft DPG
IOP Institute of Physics

Published in partnership with: Deutsche Physikalische Gesellschaft and the Institute of Physics

OPEN ACCESS

RECEIVED
15 February 2021

REVISED
16 August 2021

ACCEPTED FOR PUBLICATION
6 September 2021

PUBLISHED
29 September 2021

PAPER

Geometric signatures of tissue surface tension in a three-dimensional model of confluent tissue

Preeti Sahu[1,2,*], **J M Schwarz**[1,3] **and M Lisa Manning**[1,*]

[1] Department of Physics and BioInspired Syracuse: Institute for Material and Living Systems, Syracuse University, Syracuse, NY 13244, United States of America
[2] IST Austria, Am Campus 1, 3400 Klosterneuburg, Austria
[3] Indian Creek Farm, Ithaca, NY 14850, United States of America
[*] Authors to whom any correspondence should be addressed.

E-mail: preeti.sahu@ist.ac.at and mmanning@syr.edu

Keywords: biological tissues, 3D Voronoi model, heterotypic tension, cell sorting, demixing, topological pinning

Supplementary material for this article is available online

Abstract

In dense biological tissues, cell types performing different roles remain segregated by maintaining sharp interfaces. To better understand the mechanisms for such sharp compartmentalization, we study the effect of an imposed heterotypic tension at the interface between two distinct cell types in a fully 3D Voronoi model for confluent tissues. We find that cells rapidly sort and self-organize to generate a tissue-scale interface between cell types, and cells adjacent to this interface exhibit signature geometric features including nematic-like ordering, bimodal facet areas, and registration, or alignment, of cell centers on either side of the two-tissue interface. The magnitude of these features scales directly with the magnitude of the imposed tension, suggesting that biologists can estimate the magnitude of tissue surface tension between two tissue types simply by segmenting a 3D tissue. To uncover the underlying physical mechanisms driving these geometric features, we develop two minimal, ordered models using two different underlying lattices that identify an energetic competition between bulk cell shapes and tissue interface area. When the interface area dominates, changes to neighbor topology are costly and occur less frequently, which generates the observed geometric features.

1. Introduction

An important collective phenomenon observed in groups of biological cells is the process of cell sorting, where cells of different types spontaneously spatially segregate into separate compartments. These distinct compartments not only play an integral role during an organism's formative stages [1–5], but are also crucial for the upkeep of normal functioning of organs [6, 7] and for containment of the spread of diseased/infected tissues [8–11]. Broadly speaking, cell sorting mechanisms can be classified into two generic categories—(a) biochemical/morphogen gradients [12, 13] and (b) differences in mechanical properties of individual cells. These mechanical properties can include cell–cell adhesivity [14, 15], acto-myosin contractility [16–19], a mechano-chemical coupling between both cell–cell adhesivity and acto-myosin contractility [20–22], or an explicit interfacial tension between unlike cells, often called heterotypic interfacial tension (HIT) [23–26].

Much of the computational and theoretical work on cell sorting has focused on particle mixture simulations. In such mixtures, the mechanism for sorting relies heavily on active fluctuations [27–31]. However, an essential feature of cell sorting that is observed in experimental co-cultures is that the interface is much sharper than what is expected from a particulate mixture [21, 32–36]. While such a straight and sharp interface is difficult to obtain merely by diffusive morphogens, HITs in confluent tissues, where there are no gaps between cells, can generate a sharp interface easily [26, 37, 38]. In such cases, the fact that a confluent monolayer must tessellate space, which is captured in vertex or Voronoi models for tissues, results

in forces that are discontinuous functions of cell displacements. It is precisely this non-analytic behavior resulting from topological interactions between cells that drives sharpening in two dimensions. And yet, the tissue remains fluid-like such that the sharp interface is also easily deformable. Such sharp but deformable interfaces are not observed in particle-based models with metric interactions between cells.

While confluent monolayers, with a single layer of cells, are biologically relevant, fully three-dimensional confluent tissues, such as stratified epithelia or early vertebrate embryos, are even more ubiquitous. Therefore, it is important to determine if/how the topological nature of the interactions between the cells also drive sharp but deformable interfaces in three dimensions. Prior work on topological models for cell sorting in three dimensions focused on cells coalescing into small clusters via a Rayleigh–Plateau instability as well as regions of mixed cell types untangling to facilitate compartmentalization in the absence of fluctuations [39]. In this manuscript we instead focus on quantifying the dynamics and cell geometries in the presence of fluctuations, and identifying the topological mechanisms driving cell sorting in three dimensions.

One goal is to study the dynamics of cell sorting in confluent fluid-like tissues by implementing HIT in the presence of fluctuating forces in 3D. Indeed, we demonstrate that HIT is an efficient sorting mechanism and that, unsurprisingly, the magnitude of HIT governs the timescale for segregation in 3D.

Unfortunately, it is rather difficult to test this prediction in experiments, as it is quite difficult to measure the magnitude of HIT. In laser ablation experiments on monolayers, cuts are made to ablate a cell–cell junction with the help of a pulsed laser. The resultant relaxation dynamics can help determine line tensions [40]. However, ablating interfaces and recording retractions along arbitrary interfaces is very difficult in 3D [41], and has not been yet used to estimate HIT in 3D. Indirect measures using few-cell assays, such as double pipette aspiration experiments, suggest that HIT can create robust cell sorting in 3D tissues [6, 19, 42].

However, using isolated cells for measuring effective tension may not provide a complete picture as a confluent neighborhood can significantly change a cell's mechanics [25, 26]. Recent work has shown that geometrical properties of interfacial cells in a confluent neighborhood can be directly affected by increased interfacial contractility and tension [26, 43, 44]. Therefore, a second goal is to explore the idea that cellular geometry can perhaps be used as a simpler and more direct readout of HIT in 3D mixtures, as geometric features have recently become more accessible in experiments due to advances in tissue segmentation techniques.

In addition to developing tools for measuring HIT, a third goal of this work is to identify the mechanisms driving cell sorting in 3D. For a fluid-like particulate mixture, the mechanism is simple, as the minimum energy state is a configuration that minimizes the shared surface area. In the presence of large enough fluctuations the system can find a simple geometry that achieves this goal via complete spatial segregation with a strong gradient at the interface [45–47]. In confluent tissues, however, there are cell-scale geometric constraints that may compete with macroscopic interfacial dynamics. Specifically, in vertex and Voronoi models for isotropic confluent tissues [21, 48–56], cells attempt to attain a preferred cell shape index, which is dimensionless ratio of perimeter P and area A i.e. $s_0^{2D} = P/\sqrt{A}$ in 2D [54, 57], and of surface area S and volume V i.e. $s_0^{3D} = S/V^{2/3}$ in 3D [56].

If the cells are able to attain their preferred cell shape, which generally happens in isotropic tissues for elongated shapes with $s_0^{2D} > 3.81$ and $s_0^{3D} > 5.41$, then the tissue is fluid-like, while if they are unable to attain that shape the tissue is solid-like. Importantly, this shape-based rigidity transition appears to be a robust, universal feature of models of confluent tissues where the cells tessellate space: they occur in vertex [49, 54], Voronoi [57, 58], and cellular Potts models [59], and even appears in some models where the cells are deformable but not quite confluent [60, 61]. This indicates that a whole class of models with topological interactions, where the connectivity of neighbors that matters instead of metric distance between particles, exhibit similar energy barriers to cell rearrangements. We hypothesize that similar energy barriers affect surface-tension-driven cell rearrangements as well.

In standard fluids with metric interactions, there are many equivalent methods for measuring surface tension, which might appear at first glance to be more accessible in biology experiments than the shape-based methods proposed here. For example, in molecular fluids there is a characteristic width of the interface between two fluids, set by the magnitude of the interfacial tension.

However, previous work by some of us on 2D models [26] has demonstrated that this relationship between width and surface tension completely breaks down in both vertex and Voronoi models for confluent tissues, due to pinning effects generated at cusps in the potential energy landscape at the interface. As a result, heterotypic interfaces in confluent tissues are much sharper than expected from fluctuation–dissipation relations, and many of the traditional surface tension measurements based on capillary length scales will not work to predict HIT in 2D epithelial monolayers. Moreover, as shown below,

we are able to identify similar cusps in the landscape of the 3D Voronoi model, and so we expect similar effects persist in 3D.

In addition, these 2D results suggest specific features of the 2D cell-scale geometry help pin cells at a heterotypic interface, although it is not trivial to generalize the arguments to 3D. Therefore, we study whether these cell-scale constraints, which vary with tissue rheology, impact cell sorting in 3D. We develop simple toy models to demonstrate that a competition between the bulk cell shape preference and geometric pinning of cell shapes at the heterotypic interface drive both cell sorting and the formation of specialized geometric features at the HIT interface. Finally, we confirm the predictions made by the toy models with full numerical simulations.

2. Model

To understand the interfacial mechanics between two cell types, we use the recently developed 3D Voronoi model [56]. Similar models with slight differences in the energy functional have been used to study tissue growth [62]. A system with periodic boundaries is created using a Voronoi tessellation of the cell centers of N cells. Individual cells have preferred volumes V_0 and surface area S_0. The combination of volume incompressibility and surface area regulation due to adhesion and contractility generate a preferred cell shape index $s_0 = S_0/V_0^{2/3}$. For example, a regular bcc unit cell (truncated octahedron), has a dimensionless shape index of $s_0 \sim 5.31$ [63]. Here we set V_0 to 1. Half of the cells are tagged differently, creating a mixture of two cell types—$\beta = 1$ or $\beta = 2$, which are otherwise identical except there is heterotypic interface between cells of different type. Of course, in experimental systems there are likely mechanical differences between different cell types in addition to HIT. Here we ignore those differences to study effects driven by HIT, as our previous work in 2D suggests that sorting driven by innate mechanical differences is significantly weaker than HIT [64]. In addition to the original monodisperse energy functional, we impose an additional surface tension along the heterotypic interface. Therefore cells minimize their mechanical energy using the following dimensionless energy functional:

$$e = \sum_i \left[k_v(v_i - 1)^2 + (s_i - s_0)^2\right] + \sum_{\langle i,j\rangle} (1 - \delta_{\alpha\beta})\sigma a_{ij}, \tag{1}$$

where v_i denotes the ith cell volume and s_i denotes its surface area, non-dimensionalized by V_0. The unit of length is defined such that the average cell volume $\langle V_i\rangle$ is 1. Additionally, $k_s = K_V/K_S$ sets the ratio between volume and area stiffnesses, and is also set to unity. The second summation imposes an additional surface tension between heterotypic cells, where the sum is over all facets with area a_{ij} shared between cells i and j of types α and β respectively. The surface tension σ, for simplicity, is assumed to be the same for all facets. It is non-dimensionalized by $K_S V_0^2$ which is unity for our system. Biological cells can establish heterotypic tension by co-regulating the acto-myosin network and adhesion molecules [20]. A biologically relevant estimate of the heterotypic to homotypic tension ratio, based on examination of the contact angles at cell vertices in ectoderm–mesoderm co-cultures in Xenopus [25], indicates $\sigma \sim 2$ in natural units of the system. For systems with fluctuations, we analyze the dynamics of over-damped self-propelled particles with a high angular noise, which effectively leads to Brownian dynamics at the timescales relevant to us. The timescales are reported in units of the self-diffusivity timescale τ_s^0, details of which are provided in supplemental section S1 (https://stacks.iop.org/NJP/23/093043/mmedia). While there are other possible dynamical rules, recent work on 2D mixtures has shown that the properties of an interface between two cells types with HIT between them is rather robust to the specifics of the dynamical rules [26]. For analyzing behavior in the absence of fluctuations, we use a conjugate gradient minimizer. See supplemental section S1 for more details.

3. Results

Demixing parameter: to test if HIT leads to significant segregation in 3D tissues, in a manner similar to that of 2D mixtures [64], we first focus on a fluid-like parameter regime [56] where cells undergo diffusive motion ($s_0 > 5.41$). For a fixed shape index $s_0 = 5.5$, we start from an initially mixed configuration figure 1(a) with a system size of $N = 512$ cells. We let the system evolve long enough so each cell on average explores a distance equivalent to 5 cell lengths.

Let us now understand the role of HIT on the bulk demixing. For a fixed $\sigma = 1$, a final configuration for such a mixture is shown in figure 1(b). It is clearly segregated as compared to the initial snapshot. Some fraction of ensembles are able to create a planar interface as well. To quantify this demixing, we study the demixing parameter DP [64], which measures the average neighborhood composition of every cell.

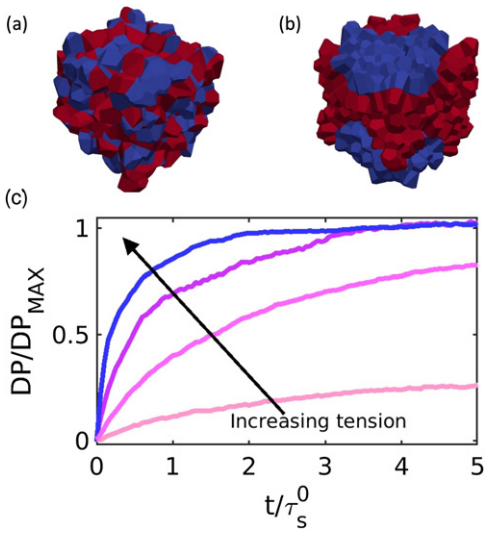

Figure 1. Sorting in fluid-like binary tissue with HIT: initial (a) and final (b) snapshots of a $s_0 = 5.5$ mixture with high tension of $\sigma = 1$ and system size of $N = 512$. Both cell types denoted by red and blue polyhedra. (c) Quantification of segregation: demixing parameter DP versus simulation time in units of self-diffusivity timescale τ_s^0 for increasing tension $\sigma = 0.001, 0.003, 0.010, 0.032$ (pink to blue).

Defining N_s as the number of homotypic (similar cell type) neighbors and N_t as the total number of neighbors,

$$\mathrm{DP} = \langle \mathrm{DP}_i \rangle = \left\langle 2\left(\frac{N_s}{N_t} - \frac{1}{2}\right)\right\rangle, \tag{2}$$

where the brackets denote averaging over all cells in the tissue. In a completely mixed state, DP = 0, whereas in a completely sorted mixture, DP = 1, in the limit of infinite system size. However, as large system sizes can be time-consuming, we compute the maximum attainable value of demixing (DP_{max}) for a particular system size by looking at minimal surface configurations as shown in figure S1. Hence we plot the demixing parameter relative to this maximum value in figure 1. The value of demixing is zero at the beginning as both the cell types are seeded at random positions, but it soon attains a high value, very close to DP_{max}. In the presence of HIT, the value of demixing increases quickly, indicating that it can efficiently create robust segregation—very similar to a liquid–liquid particulate mixture and 2D confluent mixtures.

In the presence of fluctuations, we find that HIT efficiently leads to significant segregation in mixed 3D tissues. We also observe that with higher values of tension, the initial phase of the sorting process becomes faster as shown in figure 1. This confirms that heterotypic surface tension is very effective at compartmentalization in 3D, as expected.

Geometric features: while biological cells are capable of upregulating tension cables along heterotypic interfaces via biochemical pathways, it is very difficult to directly measure this tension within a 3D tissue. Can features of individual cells at the interface help us quantify such tensions? In this section, we focus again on fluid-like systems with $s_0 = 5.5$. A visual inspection of the segregated mixture shown in figure 1(b) indicates that the interfacial cells may be more elongated and nematically ordered as compared to the cells in the interior. This observation hints at a direct relationship between the applied tension and the surrounding cellular geometry. To delve deeper into the ways in which the surrounding cells deform, we set up a maximally segregated mixture. Here, both compartments are placed side by side, similar to previous work by Sussman *et al* [26]. We then study the cellular geometry as a function of the applied interfacial tension. Shape elongation along with the prominent stacking of cells (alignment of the polyhedral long axes in figure 2(a)) can be observed here as well. We next quantify such geometric effects.

The first quantity is the steady-state cell shape index s. This helps us quantify whether or not the otherwise homogeneous cells remain homogeneous after HIT is established. We measure the shape of both interfacial cells–cells that directly touch the boundary (s_{boundary}), and the interior cells (s_{bulk}). This further helps isolate the shape changes in the immediate neighborhood of the interface. Individual cells have a final volume V_i and surface area S_i. Hence, s_{boundary} is defined as:

$$s_{\mathrm{boundary}} = \left\langle \frac{S}{V^{2/3}} \right\rangle_{\mathrm{boundary}}, \tag{3}$$

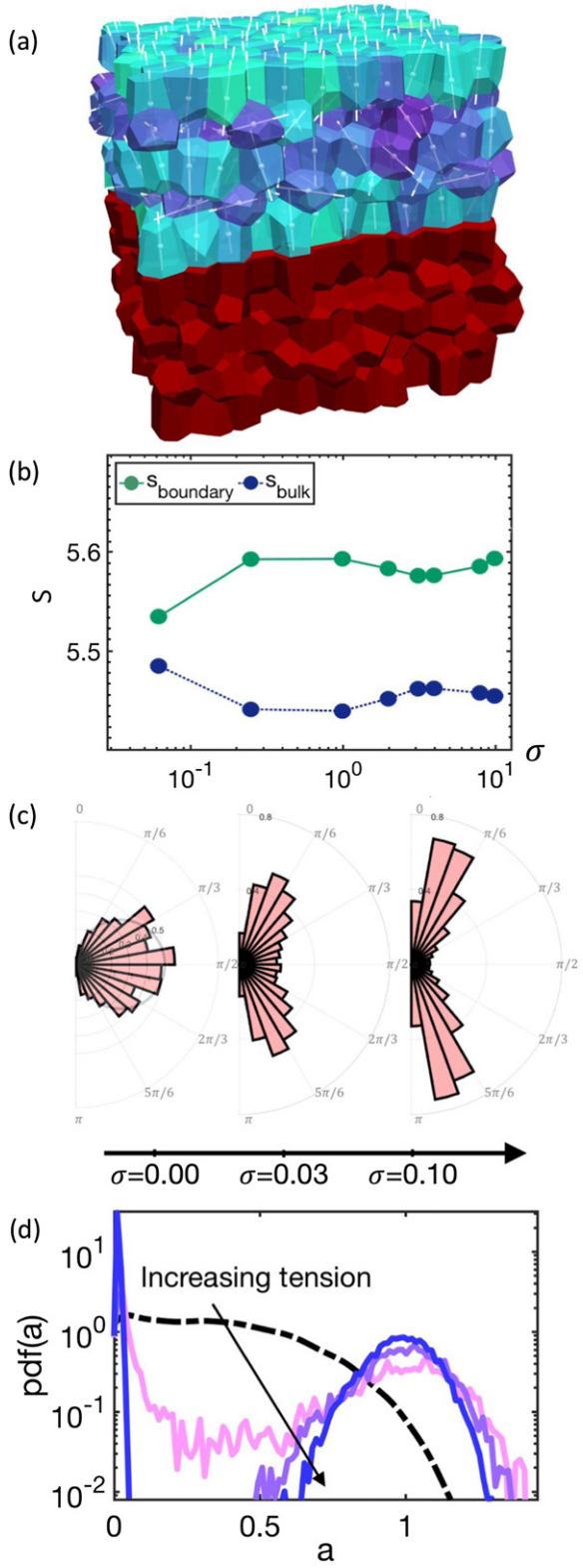

Figure 2. Cellular geometry changes around the high-tension interface: (a) snapshot of the bilayer arrangement of sorted compartments for a high value of HIT, $\sigma = 20$. Only the blue cell type is emphasized here, colored by major axis length. Greenish-blue is for elongated and purple for rounder cells. The white rods denote the long axis of the polyhedron. (b) Acquired cell shape index (s), plotted with respect to tension (σ), is higher for interfacial cells (solid green curve) as compared to the cells in bulk (dashed blue curve). (c) Rose plot for the distribution of orientation angle of interfacial cells is shown for increasing tension (σ). The control distribution ($\sigma = 0$) is superimposed on a faint black curve that represents the density for uniform distribution i.e. $\sin\theta$. (d) The probability distribution $P(a)$ of heterotypic facet area a is shown for increasing tension $\sigma = 0.32, 1.00, 2.00$ (magenta to blue). For these data, $N = 512$ and $s_0 = 5.5$.

and $s_{\rm bulk}$ is similarly averaged over the interior cells. In the absence of HIT ($\sigma = 0$), both shapes have the same value of $s_0 = 5.5$.

Both the shape indices are shown as a function of increasing tension in figure 2(b). For small values of tension, the shapes indices are very similar at the beginning, but they gradually saturate at a higher value of disparity. In other words, with a higher interfacial tension, the neighboring cells become more elongated, whereas the interior cells become more compact/round.

To study the alignment between cells, we next measure the orientation of interfacial polyhedra. We define orientation vector of a cell as the major axis of its moment of inertia tensor. We then plot the angular distribution of the angle made by each vector with respect to the normal to the interface (θ), which in this bilayer arrangement is simply the z axis. For a homogeneous system with no HIT, the angles are very close to the random distribution density function in 3D, which is proportional to $\sin\theta$. But with a slight increase in tension, the cells polarize and orient themselves perpendicular to the interface, as shown in figure 2(c).

Lastly, we study polygonal faces that make up the heterotypic interface by plotting the facet area distribution with respect to increasing tension. This is in analogy to the measurement of edge lengths in 2D work [26]. With no HIT, the distribution is roughly uniform up to a characteristic length scale, whereas, with increasing tension it becomes bimodal, as shown in figure 2(d). This means that the facets are either large or vanishingly small at high tensions. With the help of smaller facets, the interfacial vertices come very close to having a vertex coordination higher than the normal tetrahedral coordination, similar to the four-fold vertices observed along 2D tension cables. The average area of a facet, $\langle a \rangle$, also increased with increasing tension as shown in figure S2. This quantitatively confirms that HIT indeed affects the geometry of the surrounding cells, inducing shape changes and nematic-like ordering in an otherwise homogeneous collection of cells.

Since some similar geometric features have been observed in 2D models for confluent tissues [26], we hypothesize that the origin of these signatures in 3D might be based on topological interactions between the cells which have been implicated in 2D.

In order to determine the mechanism driving these geometric changes, we first focus on the specific geometry of an interfacial cell and ask: what does it take for the system to attain this precise geometry?

A typical interfacial neighborhood is shown in figure 3(a). A right prism can be defined as a polyhedron with flat top and bottom facets, and perpendicularly aligned lateral facets. The cells here seem to closely resemble the geometry of a one-sided right prism, with the flat side at the interface. The unique shape can be attained in a Voronoi tessellation only by fulfilling two conditions: (a) cell heights are arranged in a plane, and (b) interfacial pairs align their centers so the distance between centers in the XY plane is minimized. One way to quantify this alignment is to measure it as the registration—R between the cell centers. We define it as—

$$R = 1 - \frac{d}{l_0}, \tag{4}$$

where l_0 is the typical lengthscale and d is the distance between centers along the interfacial plane as depicted in figure 3(a). The value of l_0 is set to unity as $V_0^{1/3} = 1$ in our systems. When cell centers are completely registered its value attains a maximum value of unity. We quantify both of the aforementioned criteria and find them both fulfilled for higher values of tension, as shown in figures 3(b) and (c). Moreover, the insets to each figure show that the cell geometries approach the right-prism condition monotonically as a function of increasing HIT.

From work in 2D we understand that perturbations perpendicular to the surface of the interface are very costly [26], but cell–cell registration requires perturbations to the cell center that are parallel to the interface. In the SM we extend the 2D calculation to study the effects of parallel perturbations by changing the cell–cell registration. In the 2D toy model, we find that parallel perturbation incurs exactly the same energy penalty as a perpendicular perturbation up to linear order. Similar to the perpendicular perturbation, the parallel perturbation along the heterotypic interface requires the system to form new, high tension edges which are energetically very costly. Therefore, the cell centers are laterally pinned. In S5 we explore if de-registration in 3D systems creates a similar effect. We find that in an idealized hexagonal tissue, such a perturbation creates several new HIT facets, suggesting that a similar mechanism is operating in 3D.

Mechanisms: to better understand the pinning mechanism in 3D, we next develop two ordered toy models in 3D and study the response in the limit of zero fluctuations. Although the data shown so far, and work by some of us in 2D [26], focused exclusively on the fluid-like regime with $s_0^{2D} > 3.81$ and $s_0^{3D} > 5.41$, we are also interested in how tissues close to the fluid–solid transition balance interfacial and bulk effects. Therefore, our first toy model is initialized in a bcc lattice, as a ground state for the shape $s_0 \sim 5.31$. We fix $s_0 = 5.31$ to this ground state value, which we expect to be solid-like. This is similar to our recent work on ordered hexagonal monolayers [38], but here we are investigating a different form of local perturbation in 3D.

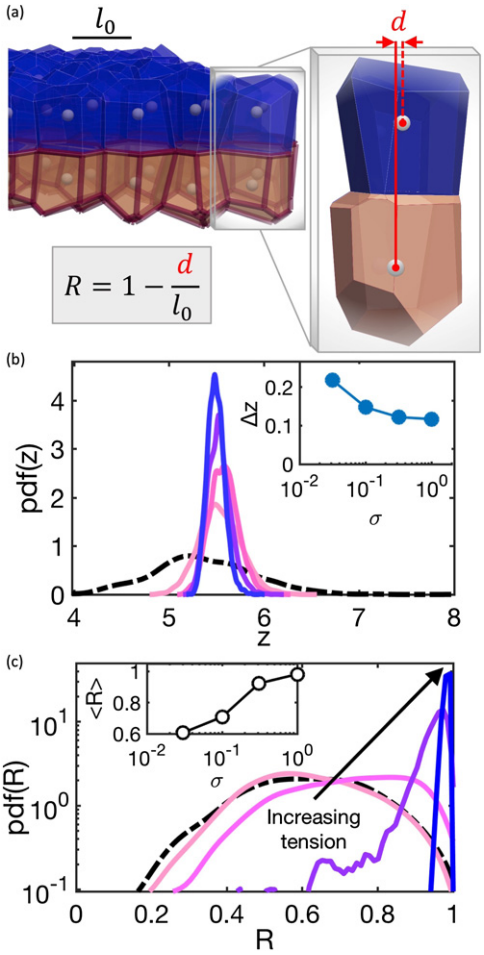

Figure 3. Interfacial cells are prism-like: (a) a simulation snapshot highlighting the cells at both sides of the interface. Cell types are tagged in blue and red and made translucent to make their centers (white solid spheres) visible. To characterize the high alignment between the heterotypic cell centers we use cell–cell registration R defined in the main text in terms of the distance d between the centers along the interface (highlighted in red) and the characteristic cell length l_0 (denoted by the black scale bar). (b) Distribution pdf(z) of the heights of cell centers z for blue interface cells is plotted for increasing tension $\sigma = 0.03, 0.10, 0.31, 1.00$ (magenta to blue). The dashed black line depicts a system with no HIT. The inset shows the standard deviation Δz with as a function of the HIT σ. (c) Distribution of registries pdf(R) between heterotypic cells is plotted for increasing tension. The inset shows the averaged registry with respect to tension. The lowest value of tension has the same average distance as no tension at all. The circle radii corresponds to the deviation from the mean values.

In this work, we study the response of the system to a change in the registry R. In these ordered systems, we now use the lattice spacing as the lengthscale l_0 in the definition for registry in equation (4). We enable a string of polyhedra to slide past the string below (shown in figure 4(a) insets), with an extra surface tension along the shared interfacial strip between both the sets of polyhedra. We compute the shared surface area and total energy of the system. We also find the global minima for different values of tension.

We find that the shared surface area is minimized for increased registration values (shown in figure 4(a)). While this suggests that perhaps complete registration is an energetically preferred state in some regimes, surprisingly, that is true only after a threshold value of tension. This can be seen by plotting the change in total energy with respect to increasing registration. One can observe two kinds of minima in the system—parabolic and 'cuspy' [26]. While the former is common in particle-based models, with a spring-like potential locally around the minima, the later has a discontinuity in its slope due to topological pinning, which is expected from a 2D calculation as discussed in S4. Physically, this means that the system experiences a steep linear rise in energy due to the formation of a new interfacial edge along the high tension cable, resulting in discontinuous pinning forces that are independent of the magnitude of perturbation, as shown in figure S6(b). The parabolic minima, on the other hand, have a continuous an linear restoring force, the slope proportional to the stiffness of the parabola. We plot the registration of energy minima as a function of interfacial tension in figure 4(c).

We observe two different branches corresponding to the two types of minima discussed before. For very low tension, shape preference dominates (as shown in figure S5(a)) and the system stays in bcc configuration. For moderate values of tension the system stays in the parabolic branch, but continuously

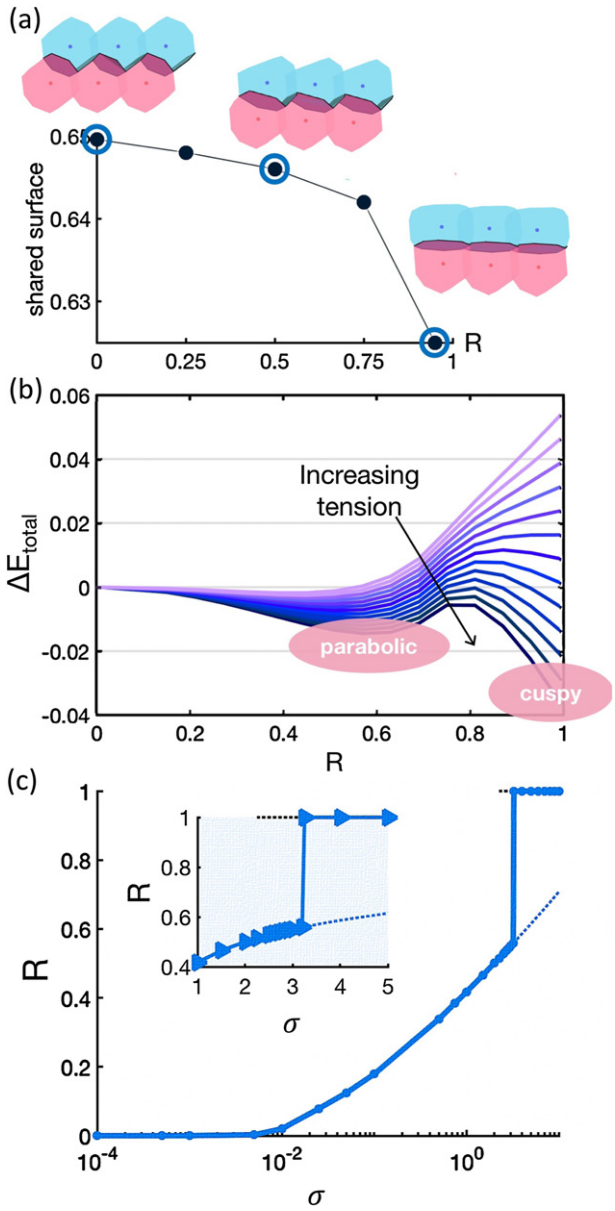

Figure 4. Global minimum becomes registered for higher tension: (a) shared surface area (shaded in dark for all snapshots) is computed as a function of the registration between the different cell types. The string of blue cells is allowed to move past the string of stationary pink cells. Snapshots for no, half and complete registration is shown for encircled points. (b) The change in the total energy of this system is plotted with respect to registry, for different values of tension ranging from 1 (pink) to 4 (blue) in increments of 0.25. (c) The ground-state registration is plotted for increasing tension. The solid curve represents the global minima. The dashed curves represent the local minima, parabolic in blue and cuspy in black. The inset zooms about the critical tension at which the transitions occurs between both types of minima. For all panels s_0 is set to 5.31, the ground state for the bcc lattice.

transitions to non-zero registry. Just below the critical value of $\sigma_c \sim 3$, both the shape and interfacial energies become comparable (figure S5(b)) and at σ_c the system discontinuously transitions to the tension-dominated—cuspy branch. The registration value also jumps to $R = 1$. This branch originates at $\sigma \sim 2$.

Both kinds of minima become more stable as the tension increases. Stability is parameterized by the curvature or stiffness for parabolic minima in figure S6(a) and by the linear slope or restoring force for the cuspy minima in figure S6(c).

In summary, for the solid-like toy model, we find that the physical mechanism that drives registration at high tension values is very similar to that of 2D systems. However, the story changes at lower values of tension where shape frustration begins to play a dominant role. This leads to minima that are partially-registered and exhibit a spring-like response to small perturbations, i.e. states are no longer topologically pinned.

In 2D studies focused exclusively on fluid-like tissues [26], only the cusp-like states were observed. This leads us to hypothesize that perhaps we observe a transition between normal, parabolic restoring forces to

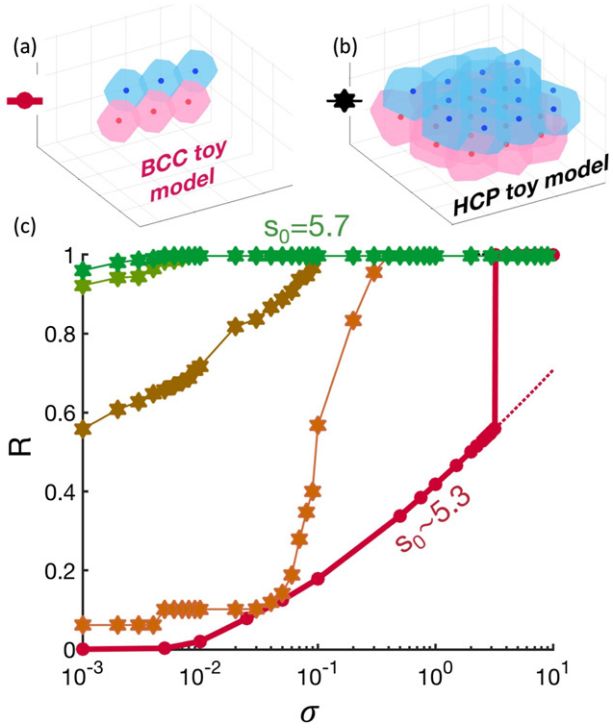

Figure 5. Shape frustration is less dominant for more fluid-like cell shapes: (a) and (b) snapshots for both the models are shown where both cell types are depicted in blue and red. Cell centers are depicted by solid spheres of respective cell color. (c) The ground-state registration for hcp toy model (filled hexagrams) is plotted with respect to tension, for increasing values of cell shape $s_0 = 5.4, 5.5, 5.6, 5.7$ from orange to green. For comparison, the registration in bcc model (solid circles) is also shown here in red.

non-analytic cusp-y restoring forces in tissues that are more solid-like. Perhaps in more fluid-like systems the interfacial costs always dominate over the cost of cell shapes in the bulk, whereas in more solid-like systems the bulk effects dominate when the interfacial tension is low.

To test this hypothesis, we develop a second toy model that is also ordered but not constrained to a string. Instead it is free to move along the 2D interface to change its registration. With this flexibility, we can explore the energetics of more elongated cell shapes like that of a uniform hexagonal prism ($s_0 \sim 5.72$). The interfacial cells can therefore be much more elongated and fluid-like as compared to the minimal-perimeter-cells in a bcc lattice that have shape values as small as $s_0 \sim 5.31$. The interfacial layers are placed in hcp format as shown in figure 5(b). There are buffer cells placed above and below the interface in a disordered fashion and are allowed to relax during the course of the perturbation.

Analogous to the previous analysis, we compute the shared surface area and change in the energy profile with respect to registration, but this time for a wide range of cell shapes across the fluid–solid transition. We find that similar to the bcc toy model, the shared surface area decreases with registration as shown in figure S7(a). For cell shapes near the rigidity transition, shape frustration plays a dominant role in the system's energy (figure S7(b)). However, it becomes negligible for more fluid-like cell shapes as shown in figure 5. This suggests that in fully disordered fluid-like systems, interfacial tension dominates shape preferences in determining interface geometry and response.

Finally, we verify the toy model predictions by first studying the geometry of disordered mechanically stable states in planar segregated HIT simulations, for different values of HIT and preferred cell shape. We let the system come to a steady state in the presence of fluctuations that can help the system find lower and lower energy metastable minima in the complex potential energy landscape.

Figure 6 shows the registration as a function of interfacial tension and target cell shape index s_0. The data demonstrate that just as in the toy models, the average registration rises rapidly to unity—its maximum value—when the interfacial tension increases above a threshold value. Moreover, for solid-like shapes the onset occurs at a higher threshold tension of order unity, while for fluid-like tissues the onset occurs when HIT is more than an order of magnitude lower than the typical tensions between homotypic cells. In the supplement, we also confirm that the highly registered states are associated with cusp-like restoring forces, highlighted in figure S8. In addition, we show that this geometric signature is not limited to Voronoi models. Cell–cell registry in two-dimensional vertex model mixtures also develop a strong preference to higher values with increasing interfacial tension as discussed in detail in supplementary

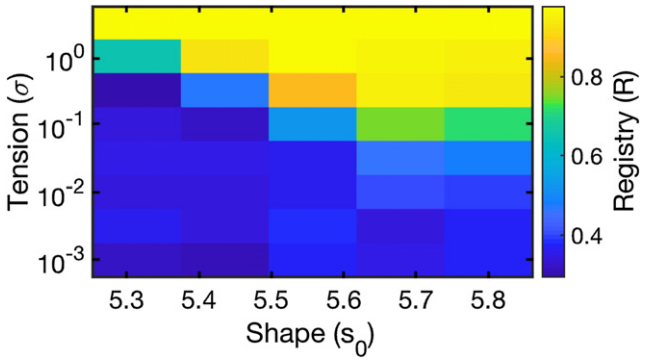

Figure 6. Transition to complete registration shifts for fluid-like cell shape in a disordered 3D simulation: a heat-map for the average steady-state registration is shown as function of cell shape s_0 and interfacial tension σ. Yellow denotes complete registration and blue denotes partial registry. The registry between heterotypic cell-pairs is averaged over 200 different initializations.

section 9. However, the magnitude of the registration saturates at a lower value in 2D vertex models (0.6 compared to 1), and also attains this saturation value at a lower value of the heterotypic tension—between 1% and 10% in 2D vertex models, rather than between 10% and 100% in 3D Voronoi models as shown in the inset to panel (C) in figure 6. In other words, the quantitative relationship between registry and the magnitude of HIT is likely model-dependent.

4. Discussion and conclusions

By studying a computational Voronoi model for confluent tissues in the presence of fluctuations, we show that three-dimensional binary mixtures, with HIT, sort robustly. This supports the claim that HIT is an important mechanism driving sharp compartmentalization during early embryonic development [25, 37], and that it may be important for tissue segregation in other situations. In addition to these collective dynamics, HIT also drives individual cells toward a prism-like geometry at the interface. We find that the onset of these geometric signatures depends on a balance between the magnitude of interfacial tension and constraints introduced by the preferred cell shape that also govern the bulk tissue rheology.

To understand the onset of these geometric signatures, we use cell–cell registration at the interface as a probe of the stability of these prism-like structures. We construct two simple toy models and study their energetics with respect to registry. In solid-like tissues, we find that for an interfacial tension $\sigma > \sigma_c$, the ground state is completely registered, which gives rise to a prismatic geometry. These states are topologically pinned, due to cusp-like pinning forces, previously observed in 2D mixtures with HIT. But for tensions $\sigma < \sigma_c$, interfacial energy is dominated by shape frustration and hence the ground state is less well-registered. The linear response of these minima is spring-like and not cuspy. Our data suggests that σ_c decreases significantly as the tissue becomes more fluid-like. This has important implications for development and tissue segregation, as it suggests that as tissues are tuned to be more solid-like, topological pinning at heterotypic interfaces is greatly reduced, thereby reducing the sharpness possible at compartment boundaries. In other words, it suggests the somewhat counterintuitive design principle for confluent systems that fluid-like rheologies lead to sharper interfaces.

We have also shown that a change in the magnitude of the interfacial tension can have a pronounced effect on the neighboring cellular geometry, by elongating interfacial cells into prism-like polyhedra oriented perpendicular to the interface. The observable facet areas also become larger. While these observed prism-like geometries have been seen in both vertex and Voronoi models [26], the registry associated with such shapes differs between vertex and voronoi models. In 3D Voronoi models, the registry varies from zero to unity over a wide range of tension values (from 10^{-3} to 10 times the average homotypic interfacial tension), but in 2D vertex models, the registry varies less—from 0 to 0.6—and attains this saturated value at lower heterotypic tensions, between 10^{-2} to 10^{-1}. In other words, the relationship between registry and heterotypic tension depends on which model best describes a given tissue. Some tissues appear to be well-described by a Voronoi model [65] and should follow registry predictions in figure 6, while others are likely best described by vertex models. In those latter systems, if one observes a registry that is at the saturation value ($\langle R \rangle \sim 0.6$), this is a good indicator that HITs above a certain threshold (1%–10%) are active in the system, so registry can likely still be used to verify HIT in those co-cultures, but can not be used to constrain the magnitude. Nevertheless, with the advancement of 3D segmentation techniques

[66–70], one can use the prism-like shape signatures as a toolkit to probe interfacial tensions in a 3D tissue, so that cells themselves can tell us about whether HIT is driving tissue segregation.

One example case where this might be useful is in detecting the invasiveness of a carcinoma tumor. Our simple model would predict that if interfacial cell centers in the tumor are registered to those of the surrounding healthy tissue, then the interface has a higher surface tension and therefore it may be more unlikely for cells to exit the tumor and invade their surroundings. It would be interesting to see if there are any vestiges of this prediction that occur in pre-cancerous situations in real-world systems, such as Ductal carcinoma *in situ* (DCIS).

Another example is that of a stratified epithelium, where one can also study the interaction between two nearby tissue types, such as the basal and suprabasal layers, and look for geometric signatures across the interface. A prism-like geometry would strongly suggest the presence of an interfacial tension between these two tissue types. The prism-like geometry of cells can be visually detected using the En Face imaging technique [6, 71]. As some current segmentation algorithms can also make predictions about 3D shape from random 2D cross-sections, these geometric signatures could potentially be characterized along the cross-sections [72]. In general 3D tissue have complex interfacial geometries. Hence, one of the future avenues of this work would be to study the dependence on the curvature of the interface.

Additional work should also focus on teasing apart how topological pinning affects dynamics in more general scenarios. For example, a natural extension of our general framework is to study two different cell shapes mixed together. After all, in realistic situations cells of two different tissue types likely also differ in preferred cell shape. In 2D, some of us have determined that unique extrusion behavior can emerge due to differential pinning of cells [64], and something similar could occur in 3D. Topological pinning might be affecting the cell sorting dynamics as well. Presumably, less pinning can lead to seamless coarsening of nearby droplets, while more pinning can hinder the coalescence, and alter the sorting process. This would also be an interesting avenue for future study.

While our work demonstrates that changes to individual cellular geometries are a necessary consequence of HIT and tissue-scale segregation, these changes to cellular geometry could also be used as a signal to facilitate downstream patterning near interfaces. For example, the elongation of cells near a high-tension interface might trigger oriented cell divisions along the long-axis of these cells. We speculate that perhaps biology can make use of this subtle feedback for processes like targeted cellular proliferation during early phases of embryonic development.

Acknowledgment

We thank Paula Sanematsu, Matthias Merkel, Daniel Sussman, Cristina Marchetti and Edouard Hannezo for helpful discussions, and M Merkel for developing and sharing the original version of the 3D Voronoi code. This work was primarily funded by NSF-PHY-1607416, NSF-PHY-2014192 , and are in the division of physics at the National Science Foundation. PS and MLM acknowledge additional support from Simons Grant No. 454947.

Data availability statement

The data that support the findings of this study are available upon reasonable request from the authors.

References

[1] Trinkaus J P and Groves P W 1955 Differentiation in culture of mixed aggregates of dissociated tissue cells *Proc. Natl Acad. Sci.* **41** 787–95
[2] Waites W, Cavaliere M, Cachat E, Danos V and Davies J A 2018 An Information-Theoretic Measure for Patterning in Epithelial Tissues *IEEE Access* **6** 40302–12
[3] Unbekandt M and Davies J A 2010 Dissociation of embryonic kidneys followed by reaggregation allows the formation of renal tissues *Kidney Int.* **77** 407–16
[4] Montero J A, Carvalho L, Wilsch-Bräuninger M, Kilian B, Mustafa C and Heisenberg C P 2005 Shield formation at the onset of zebrafish gastrulation *Development* **132** 1187–98
[5] Klopper A V, Krens G, Grill S W and Heisenberg C P 2010 Finite-size corrections to scaling behavior in sorted cell aggregates *Eur. Phys. J.* E **33** 99–103
[6] Rübsam M *et al* 2017 E-cadherin integrates mechanotransduction and EGFR signaling to control junctional tissue polarization and tight junction positioning *Nat. Commun.* **8** 1250
[7] Cochet-Escartin O, Locke T T, Shi W H, Steele R E and Collins E M S 2017 Physical mechanisms driving cell sorting in hydra *Biophys. J.* **113** 2827–41
[8] Friedl P, Hegerfeldt Y and Tusch M 2004 Collective cell migration in morphogenesis and cancer *Int J Dev Biol.* **4** 441-9
[9] Foty R A and Steinberg M S 2005 The differential adhesion hypothesis: a direct evaluation *Dev. Biol.* **278** 255–63

[10] Pawlizak S et al 2015 Testing the differential adhesion hypothesis across the epithelial-mesenchymal transition New J. Phys. 17 091001
[11] Song W, Tung C-K, Lu Y-C, Pardo Y, Wu M, Das M, Kao D-I, Chen S and Ma M 2016 Dynamic self-organization of microwell-aggregated cellular mixtures Soft Matter 12 5739
[12] Turing A M 1990 The chemical basis of morphogenesis Bull. Math. Biol. 52 153–97
[13] Streichan S J, Lefebvre M F, Noll N, Wieschaus E F and Shraiman B I 2018 Global morphogenetic flow is accurately predicted by the spatial distribution of myosin motors Elife 7 e27454
[14] Steinberg M S 1963 Reconstruction of tissues by dissociated cells Science 141 401–8
[15] Steinberg M S 2007 Differential adhesion in morphogenesis: a modern view Curr. Opin. Genet. Dev. 17 281–6
[16] Harris A K 1976 Is cell sorting caused by differences in the work of intercellular adhesion? A critique of the Steinberg hypothesis J. Theor. Biol. 61 267–85
[17] Wayne Brodland G 2002 The differential interfacial tension hypothesis (DITH): a comprehensive theory for the self-rearrangement of embryonic cells and tissues J. Biomech. Eng. 124 188–97
[18] Mertz A F, Banerjee S, Che Y, German G K, Xu Y, Hyland C, Cristina Marchetti M, Horsley V and Dufresne E R 2012 Scaling of traction forces with the size of cohesive cell colonies Phys. Rev. Lett. 108 198101
[19] Maître J L, Berthoumieux H, Krens S F G, Salbreux G, Jülicher F, Paluch E and Heisenberg C P 2012 Adhesion functions in cell sorting by mechanically coupling the cortices of adhering cells Science 80 253–6
[20] Amack J D and Lisa Manning M 2012 Knowing the boundaries: extending the differential adhesion hypothesis in embryonic cell sorting Science 338 212–5
[21] Lisa Manning M, Foty R A, Steinberg M S and Maria Schoetz E 2010 Coaction of intercellular adhesion and cortical tension specifies tissue surface tension Proc. Natl Acad. Sci. USA 107 12517–22
[22] Engl W, Arasi B, Yap L L, Thiery J P and Viasnoff V 2014 Actin dynamics modulate mechanosensitive immobilization of E-cadherin at adherens junctions Nat. Cell Biol. 16 584–91
[23] Graner F and Glazier J A 1992 Simulation of biological cell sorting using a two-dimensional extended Potts model Phys. Rev. Lett. 69 213–6
[24] Barton D L, Henkes S, Weijer C J and Sknepnek R 2017 Active vertex model for cell-resolution description of epithelial tissue mechanics PLoS Comput. Biol. 13 e1005569
[25] Canty L, Zarour E, Kashkooli L, François P and Fagotto F 2017 Sorting at embryonic boundaries requires high heterotypic interfacial tension Nat. Commun. 8 157
[26] Sussman D M, Schwarz J M, Cristina Marchetti M and Lisa Manning M 2018 Soft yet sharp interfaces in a vertex model of confluent tissue Phys. Rev. Lett. 120 058001
[27] Flenner E, Janosi L, Barz B, Neagu A, Forgacs G and Kosztin I 2012 Kinetic Monte Carlo and cellular particle dynamics simulations of multicellular systems Phys. Rev. E 85 031907
[28] Merks R M H and Glazier J A 2005 A cell-centered approach to developmental biology Physica A 352 113–30
[29] Sun Y and Wang Q 2013 Modeling and simulations of multicellular aggregate self-assembly in biofabrication using kinetic Monte Carlo methods Soft Matter 9 2172
[30] Jiang Y, Levine H and Glazier J 1998 Possible cooperation of differential adhesion and chemotaxis in mound formation of Dictyostelium Biophys. J. 75 2615–25
[31] Palsson E 2008 A 3D model used to explore how cell adhesion and stiffness affect cell sorting and movement in multicellular systems J. Theor. Biol. 254 1–13
[32] Landsberg K P, Farhadifar R, Ranft J, Umetsu D, Widmann T J, Bittig T, Said A, Jülicher F and Dahmann C 2009 Increased cell bond tension governs cell sorting at the Drosophila anteroposterior compartment boundary Curr. Biol. 19 1950–5
[33] Dahmann C, Oates A C and Brand M 2011 Boundary formation and maintenance in tissue development Nat Rev Genet 12 43–55
[34] Nnetu K D, Knorr M, Käs J and Zink M 2012 The impact of jamming on boundaries of collectively moving weak-interacting cells New J. Phys. 14 115012
[35] Monier B, Pélissier-Monier A and Sanson B 2011 Establishment and maintenance of compartmental boundaries: Role of contractile actomyosin barriers Cell. Mol. Life Sci. 68 1897–910
[36] Calzolari S, Terriente J and Pujades C 2014 Cell segregation in the vertebrate hindbrain relies on actomyosin cables located at the interhombomeric boundaries EMBO J. 33 686–701
[37] Kesavan G, Machate A, Hans S and Brand M 2020 Cell-fate plasticity, adhesion and cell sorting complementarily establish a sharp midbrain-hindbrain boundary Development 147 186882
[38] Sahu P, Kang J, Erdemci-Tandogan G and Lisa Manning M 2020 Linear and nonlinear mechanical responses can be quite different in models for biological tissues Soft Matter 16 1850–6
[39] Hutson M S, Brodland G W, Yang J and Viens D 2008 Cell sorting in three dimensions: topology, fluctuations, and fluidlike instabilities Phys. Rev. Lett. 101 148105
[40] Sugimura K, Lenne P F and Graner F 2016 Measuring forces and stresses *in situ* in living tissues Development 143 186–96
[41] Veldhuis J H, Ehsandar A, Maître J L, Hiiragi T, Cox S and Wayne Brodland G 2017 Inferring cellular forces from image stacks Phil. Trans. R. Soc. B 372 20160261
[42] Tsai T Y-C, Sikora M, Xia P, Colak-Champollion T, Knaut H, Heisenberg C-P and Megason S G 2020 An adhesion code ensures robust pattern formation during tissue morphogenesis Science 370 113–6
[43] Okuda S, Inoue Y and Adachi T 2015 Three-dimensional vertex model for simulating multicellular morphogenesis Biophys. Physicobiol. 12 13–20
[44] Yang J and Wayne Brodland G 2009 Estimating interfacial tension from the shape histories of cells in compressed aggregates: a computational study Ann. Biomed. Eng. 37 1019–27
[45] Canongia Lopes J N 2002 Microphase separation in mixtures of Lennard-Jones particles Phys. Chem. Chem. Phys. 4 949–54
[46] Majumder S and Das S K 2011 Universality in fluid domain coarsening: the case of vapor-liquid transition Europhys. Lett. 95 46002
[47] Chremos A, Nikoubashman A and Panagiotopoulos A Z 2014 Flory–Huggins parameter χ, from binary mixtures of Lennard-Jones particles to block copolymer melts J. Chem. Phys. 140 054909
[48] Nagai T and Honda H 2001 A dynamic cell model for the formation of epithelial tissues Phil. Mag. B 81 699–719
[49] Farhadifar R, Röper J-C, Aigouy B, Eaton S and Jülicher F 2007 The influence of cell mechanics, cell–cell interactions, and proliferation on epithelial packing Curr. Biol. 17 2095–104

[50] Teleman A A, Hufnagel L, Rouault H, Shraiman B I and Cohen S M 2007 On the mechanism of wing size determination in fly development *Proc. Natl Acad. Sci.* **104** 3835–40
[51] Staple D B, Farhadifar R, Röper J-C, Aigouy B, Eaton S and Jülicher F 2010 Mechanics and remodelling of cell packings in epithelia *Eur. Phys. J.* E **33** 117–27
[52] Hilgenfeldt S, Erisken S and Carthew R W 2008 Physical modeling of cell geometric order in an epithelial tissue *Proc. Natl Acad. Sci.* **105** 907–11
[53] Chiou K K, Hufnagel L and Shraiman B I 2012 Mechanical stress inference for two dimensional cell arrays *PLoS Comput. Biol.* **8** e1002512
[54] Bi D, Lopez J H, Schwarz J M and Manning M L 2015 A density-independent rigidity transition in biological tissues *Nat. Phys.* **11** 1074–9
[55] Fletcher A G, Osterfield M, Baker R E and Shvartsman S Y 2014 Vertex models of epithelial morphogenesis *Biophysical J.* **106** 2291–304
[56] Merkel M and Lisa Manning M 2018 A geometrically controlled rigidity transition in a model for confluent 3D tissues *New J. Phys.* **20** 022002
[57] Bi D, Yang X, Cristina Marchetti M and Lisa Manning M 2016 Motility-driven glass and jamming transitions in biological tissues *Phys. Rev.* X **6** 021011
[58] Sussman D M and Merkel M 2018 No unjamming transition in a Voronoi model of biological tissue *Soft Matter* **14** 3397–403
[59] Chiang M and Marenduzzo D 2016 Glass transitions in the cellular Potts model *Europhys. Lett.* **116** 28009
[60] Kim S, Pochitaloff M, Stooke-Vaughan G A and Campàs O 2021 Embryonic tissues as active foams *Nat. Phys.* **17** 859–66
[61] Loewe B, Chiang M, Marenduzzo D and Marchetti M C 2020 Solid–liquid transition of deformable and overlapping active particles *Phys. Rev. Lett.* **125** 038003
[62] Katira P, Zaman M H and Bonnecaze R T 2012 How changes in cell mechanical properties induce cancerous behavior *Phys. Rev. Lett.* **108** 028103
[63] Lucarini V 2009 Three-dimensional random Voronoi tessellations: from cubic crystal lattices to Poisson point processes *J. Stat. Phys.* **134** 185–206
[64] Sahu P *et al* 2020 Small-scale demixing in confluent biological tissues *Soft Matter* **16** 3325–37
[65] van Drongelen R, Vazquez-Faci T, Huijben T A P M, van der Zee M and Idema T 2018 Mechanics of epithelial tissue formation *J. Theor. Biol.* **454** 182–9
[66] Khan Z, Wang Y C, Wieschaus E F and Kaschube M 2014 Quantitative 4D analyses of epithelial folding during Drosophila gastrulation *Development* **141** 2895–900
[67] Stegmaier J, Amat F, Lemon W C, McDole K, Wan Y, Teodoro G, Mikut R and Keller P J 2016 Real-time three-dimensional cell segmentation in large-scale microscopy data of developing embryos *Dev. Cell* **36** 225–40
[68] Browet A, De Vleeschouwer C, Jacques L, Mathiah N, Saykali B and Migeotte I 2016 Cell segmentation with random ferns and graph-cuts *Proc. Int. Conf. Image Process. ICIP*
[69] Fernández-de Manúel L, Díaz-Díaz C, Jiménez-Carretero D, Torres M and Montoya M C 2017 ESC-track: a computer workflow for 4D segmentation, tracking, lineage tracing and dynamic context analysis of ESCs *Biotechniques* **62** 215–22
[70] Morales-Navarrete H *et al* 2019 Liquid-crystal organization of liver tissue *Elife* **8** e44860
[71] Yokouchi M, Atsugi T, Van Logtestijn M, Tanaka R J, Kajimura M, Suematsu M, Furuse M, Amagai M and Kubo A 2016 Epidermal cell turnover across tight junctions based on Kelvin's tetrakaidecahedron cell shape *Elife* **5** e19593
[72] Sharp T A, Merkel M, Manning M L and Liu A J 2019 Inferring statistical properties of 3D cell geometry from 2D slices *PLoS One* **14** e0209892
[73] Marchetti M C, Joanny J F, Ramaswamy S, Liverpool T B, Prost J, Rao M and Simha R A 2013 Hydrodynamics of soft active matter *Rev. Mod. Phys.* **85** 1143–89
[74] Sussman D M 2017 cellgpu: massively parallel simulations of dynamic vertex models *Comput. Phys. Commun.* **219** 400–6